Kinetics of Thermal Degradation of Polysulfone/Polyimide Blended Polymeric Membranes

Sikander Rafiq,[1] Zakaria Man,[1] Saikat Maitra,[2] Nawshad Muhammad,[1] Farooq Ahmad[3]

[1]*Chemical Engineering Department, Universiti Teknologi PETRONAS, 31750 Tronoh, Perak, Malaysia*
[2]*Ceramic Engineering Division, Government College of Engineering and Ceramic Technology, 73, A. C. Banerje Lane, Kolkata 700010, India*
[3]*Chemical Engineering Department, King Khalid University, Abha 61411, Kingdom of Saudi Arabia*

Received 22 July 2010; accepted 23 April 2011
DOI 10.1002/app.34862
Published online 28 September 2011 in Wiley Online Library (wileyonlinelibrary.com).

ABSTRACT: Flat-sheet asymmetric polysulfone (PSF)/polyimide (PI) blended membranes were fabricated by a phase-inversion technique. The fabricated membranes were characterized by Fourier transform infrared spectroscopy, differential scanning calorimetry, and field emission scanning electron microscopy analyses. The kinetics of thermal degradation of the membranes were studied from thermogravimetric data following Friedman's kinetic approach. The thermal degradation process of the membranes followed first-order rate kinetics, and the activation energy of the thermal degradation process increased with increasing PI content of the membrane compositions. © 2011 Wiley Periodicals, Inc. J Appl Polym Sci 123: 3755–3763, 2012

Key words: activation energy; blends; degradation; membranes; thermogravimetric analysis (TGA)

INTRODUCTION

Polysulfones (PSFs) are basically a family of amorphous, thermoplastic engineering polymers containing different functional groups, such as phenylene, sulfone, and ether groups, in their main chains. This class of polymers possesses many important engineering properties. These include outstanding chemical and thermal stability, superb strength, and lithiness. They also possess a relatively higher glass-transition temperature (T_g) and the ability to form high-quality polymeric films. These important properties make these materials suitable for the fabrication of superior-grade semipermeable membranes[1–6] for different applications. Again, aromatic polyimides (PIs) also belong to the family of high-performance glassy polymers and have a relatively higher thermal stability, excellent chemical stability, and a high T_g and dielectric constant. It has also attracted sufficient attention from researchers in separation technology as a membrane material.[7–12]

An understanding of the thermal degradation behavior of these polymeric membranes is quite important for different separation processes at elevated temperatures. Many works have been reported on the thermal behavior of polymeric materials to assess their suitability as membranes, and some of these important works are mentioned in the following text.

Lisa et al.[13] studied the thermal behavior of polystyrene, PSF, and their derivatives. They assessed the influence of the chemical structure of these polymers on their thermal stability by dynamic thermogravimetric analysis (TGA) under air. Bormashenko et al.[14] worked on the thermal degradation of thermosetting and thermoplastic polymers induced by laser radiation and studied it by Fourier transform infrared (FTIR) spectroscopy. Adamczak et al.[15] studied the thermal degradation of high-temperature fluorinated PI and its carbon fiber composites. Ren et al.[16] investigated the thermal degradation of the PI Fluorine-containing polyimide (PIF2) synthesized from 4,4′-(hexafluoroisopropylidene) diphthalic dianhydride and 4,4′-diaminodiphenylmethane by high-resolution pyrolysis gas chromatography/mass spectrometry, TGA, and FTIR spectroscopy. Totu et al.[17] studied the thermal behavior of some PI membranes and presented their results as related to the influence of the plasticizer on the thermal stability of some PI membranes using a nonisothermal kinetic investigation of the decomposition reactions. Large et al.[18] studied the kinetics of the thermal decomposition of Nafion membranes by means of high-resolution and constant-heating-rate thermogravimetry (TG) under nitrogen and a synthetic air atmosphere using Kissinger's method. They observed that the decomposition temperature of Nafion membranes were lower than that of polytetrafluoroethylene homopolymer and that the decomposition of acid

Correspondence to: S. Maitra (maitrasaikat@rediffmail.com).
Contract grant sponsors: Universiti Teknologi PETRONAS.

Nafion was more complex than that of alkali-exchanged Nafion because of the high water content in the former. Molnar et al.[19] studied the thermal stability of some novel PSF derivatives by TG. They identified the thermal decomposition products by various coupled mass spectrometric methods and deduced the possible decomposition mechanism from these data. Li and Huang[20] studied the thermal degradation and kinetics of bisphenol A PSF by high-resolution TG. They observed that the thermal degradation temperature of the PSF increased slightly with an increase in the heating rate. The activation energies (E_a's) of thermal degradation of PSF in air, nitrogen, and argon atmospheres were found to be 140, 258, and 293 kJ/mol, respectively. Li and Huang[20] also observed that E_a of thermal degradation calculated by high-resolution TG in nitrogen and air were almost the same as those measured by traditional isothermal or constant-heating-rate TG.

In this work, PSF–PI blended asymmetric membranes with different compositions were fabricated by phase-inversion techniques. The kinetics of thermal degradation of the polymeric blends were studied under dynamic conditions by TG at multiple heating rates. E_a's of thermal decomposition of these polymeric blends were determined as a function of the polymeric composition from the kinetic analyses following Friedman's isoconversional kinetic approach.[21]

EXPERIMENTAL

Materials

PSF Udel P-1800 (T_g 185°C) in pulverized form was purchased from PSF is from Solvay Advanced Polymers, L.L.C, Alpharetta, Georgia, U.S.. Powdered PI Matrimid 5218, with the monomers 3,3′,4,4′-benzophenone tetracarboxylic dianhydride and diaminophenylindane (T_g 302°C), was supplied by Huntsman Advanced Materials Americas, Inc. Dichloromethane (DCM; 99%, Merck, bp = 40°C), *N*-methyl-2-pyrrolidone (NMP; 99%, Merck, bp = 204.3°C), and ethanol (99.8%, Merck) were used as organic solvents to prepare films by solution casting.

Membrane preparation

Both of the polymers were dried at 110°C for 8 h before use. The casting solution was prepared from 25 g of a total dope solution to develop membranes of different compositions. The relative proportions of PSF and PI in the batch compositions are shown in Table I. The solution was stirred gently (to prevent the formation of bubbles in the casting solution) in a round-bottom vessel for 24 h at 35°C to prepare a clear solution.

TABLE I
Compositions of the Fabricated PSF–PI Membranes

Membrane sample	Membrane blend		Membrane thickness (μm)	T_g (°C)
	PSF (%)	PI (%)		
1	100	0	39.845	185.33
2	0	100	38.967	302.91
3	95	5	40.245	190.85
4	90	10	35.852	198.67
5	85	15	41.215	204.77
6	80	20	35.525	209.09

The solution was further ultrasonically degassed with an ultrasonic water bath (Transsonic Digital S, Elma, Germany). The clear solution obtained was used to cast membranes by a doctor's blade technique with an opening gap of 150 μm. Phase inversion was carried out to develop the membrane from the liquid gel mass with ethanol as a coagulation medium.

Field emission scanning electron microscopy (FESEM)

The morphology of each membrane was analyzed by FESEM (Carl Zeiss model SUPRA 55VP) Oberkochen, Germany. Random specimens from the fabricated asymmetric membranes were drawn carefully with a sharp blade to examine the morphology of the surfaces. Cross sections of the membranes were cryogenically obtained by liquid nitrogen fracturing to get clear images of the sections. The samples were then gold-coated by sputtering under a Polaron Range SC7640.

FTIR spectroscopy

To measure the molecular interactions between the polymers in the blends, a drop from each different dope solution was pelletized under a pressure of 1000 psi with potassium bromide. The thin polymer-coated pellets were dried *in vacuo*. FTIR spectra for the samples were taken with a PerkinElmer FTIR spectrometer (Spectrum One), Buckinghamshire, England in the 500–2000-cm^{-1} wave-number region.

Differential scanning calorimetry (DSC)

To determine T_g of the blended membranes, the samples were cut into small pieces having approximately 10 mg of weight. The thermal scans of the samples were carried out from 100 to 350°C with a heating rate of 10°C/min under a nitrogen atmosphere with a PerkinElmer DSC Pyris-1 calorimeter.

TGA

The thermal stability of the membranes was investigated with a PerkinElmer TGA-7 apparatus. Thermal

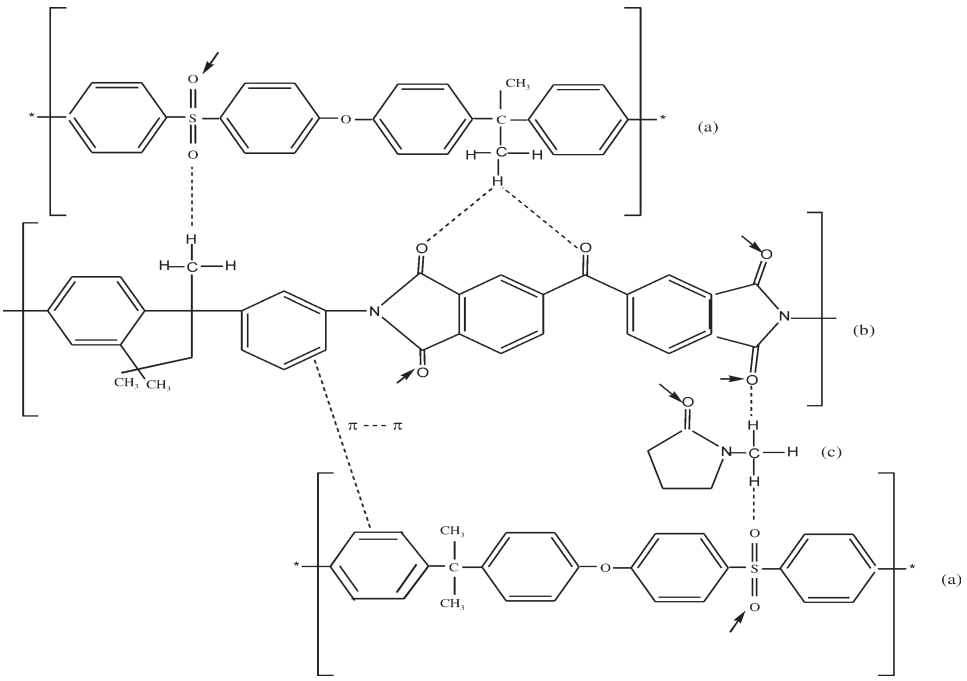

Figure 1 Interaction between (a) PSF, (b) PI, and (c) NMP. The dotted lines and arrows indicate the probable site for hydrogen-bond formation with amine groups in other molecules.

scans of samples weighing approximately 10 mg were run from room temperature to 700°C at three different heating rates of 5, 10, and 15°C/min in liquid nitrogen at 20 mL/min.

RESULTS AND DISCUSSION

Asymmetric polymeric membranes were fabricated by a phase-inversion technique with different proportions of PI and PSF. In the solvent mix, DCM was used as the solvent, and NMP in the casting solution controlled the rate of evaporation. The schematic diagram of the interaction of polymeric units in the solvents is presented in Figure 1. The solvents facilitated the dissolution process of the polymers, PSF, and PI through H bonding. During the fabrication process, the low-boiling solvent DCM facilitated the development of diffused skin layer by its rapid rate of evaporation, which left behind the residue. NMP, on the other hand, controlled the rate of solvent evaporation from the system because of its relatively higher boiling nature.

From Table I, it can be seen that with the increase in the PI content, the thickness of the membrane did not change uniformly. As the total polymer content remained the same in all of the batches, this irregular change in thickness in the batches could be related to the complex interaction between the polymers. The thickness of the membranes was maintained in the range 35–41 μm.

From the microstructures [Fig. 2(a–c)] of the PSF and blended membranes, it is apparent that the membrane surfaces were reasonably homogeneous. This could be related to the adequate compatibility of the two glassy polymers. The polymeric blends apparently showed no phase separation. The individual surfaces of PSF and PI showed interconnected dead-end pores of different sizes and population densities. However, these type of pores were absent in the PSF/PI-20% membrane, making the membrane surface for this composition comparatively more homogeneous. The cross-sectional views of the membranes [Fig. 2(d,e)] showed the presence of fairly dense skins and porous sublayers in the structures, and hence, by definition, it could be described as an asymmetric membrane.[22] The development of the skin layer can be related to the proper control of dry and wet processes during the fabrication of a membrane. In the liquid phase, the coagulation process was quite fast at the surface of the membrane. This resulted in the rapid gelling of the polymeric molecules onto the surface, which formed a thin skin layer. Once formed, the skin layer continued to increase in area until the diffusion of ethanol (nonsolvent) from the sublayer of the membrane through the skin layer was completely stopped.[23] For flat-sheet membranes, an evaporation time of 10–15 s was observed to be suitable for the development of a defect-free top skin layer.[24] Therefore, in this study, an evaporation time of 15 s was maintained. Hence, relatively thinner skin layers with thick subporous structures were observed for the membrane under the experimental conditions. Thin skin layers with dense porous supports at the bottom have been

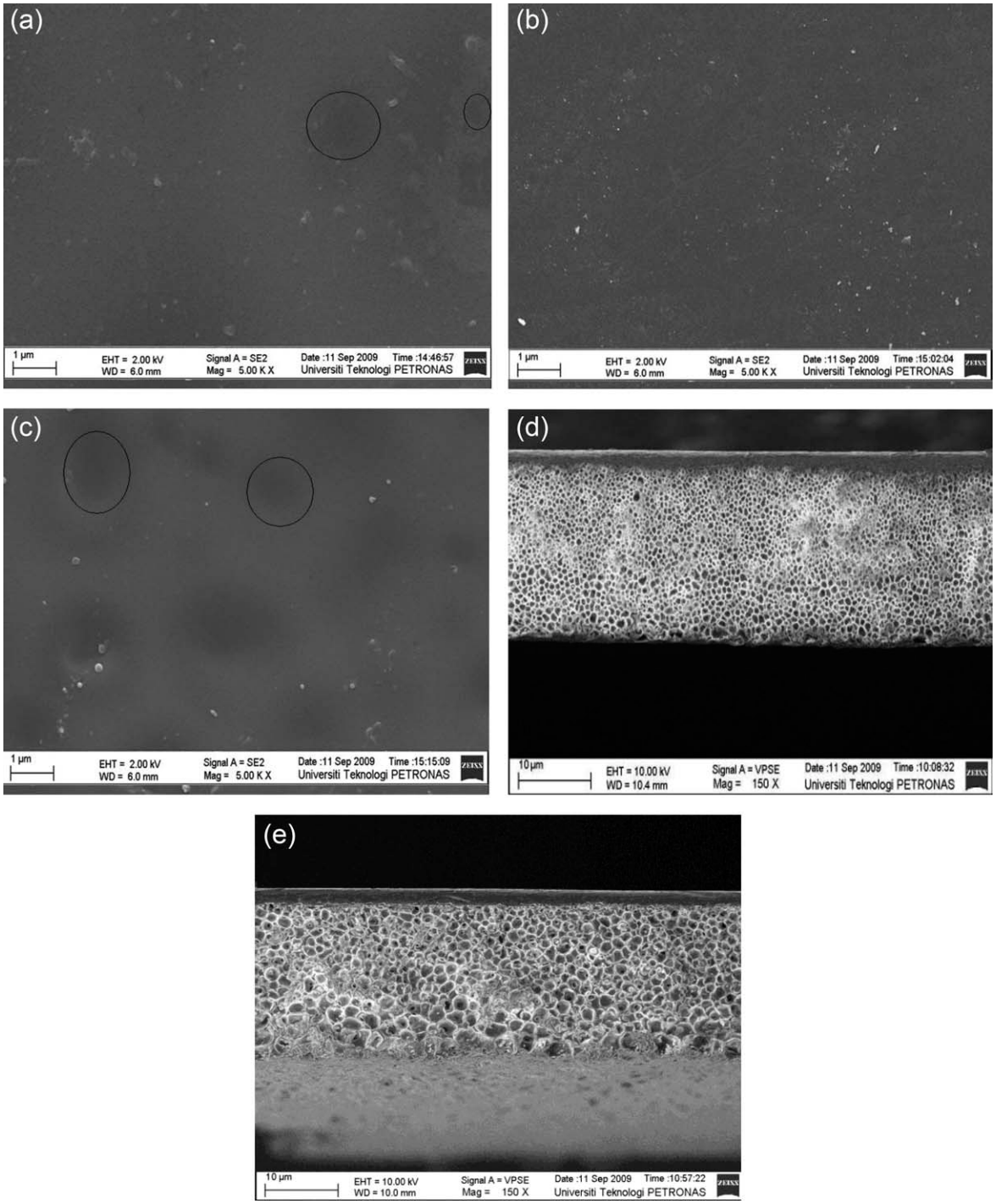

Figure 2 FESEM images of the surfaces of (a) PSF, (b) PSF/PI-20%, and (c) PI and cross sections of (d) PSF and (e) PSF/PI-20%.

observed to be quite suitable for gas-separation applications.[25,26] Microstructures of these types of membranes reveal spongelike structures rather than fingerlike macrovoids in the subporous layer; this indicates the absence of defects and pinholes at the membrane surfaces.[22] The microvoids in the membrane substructure could be reduced with the addition of PI in the PSF membrane. However, an examination of the cross sections of the membranes revealed that the concentration of PI increased at the expense of PSF in the dope solution.[27] So at a constant polymer concentration, the thermal stability effects were examined with regard to the addition of PI.

The T_g values from the DSC curves for the PSF/PI blended membranes are shown in Table I. The miscibility of the polymers at the molecular level was confirmed by DSC experiments, as all of the

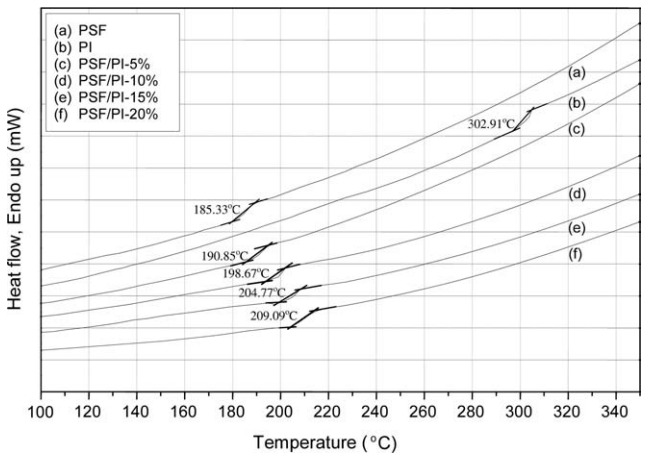

Figure 3 DSC thermograms of the PSF, PI, and PSF/PI membrane blends.

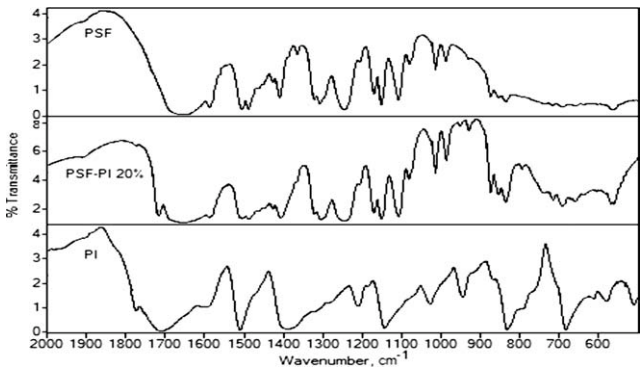

Figure 4 Comparative FTIR spectra of the PSF, PI, and PSF/PI-20% membranes.

compositions exhibited distinct single T_g values. Also, for these PSF/PI blends of various compositions, no phase separation was observed; this was also consistent with past studies.[28] The T_g values of samples for pure and blended membranes were taken as the midpoints of the heat flow versus temperature curves. Pure PSF and PI were found to be at their characteristic T_g values of 185.33 and 302.91°C, respectively. Although for membrane blends, we observed that with the increase in PI content, the T_g of the polymeric blend increased (Fig. 3).

The FTIR spectra of PSF, PI, and PSF/PI-20% blended asymmetric membranes are shown in Figure 4. For PSF, symmetric and asymmetric vibrations associated with S=O were found at wave numbers of 1150 and 1307 cm^{-1}, respectively. C—SO_2—C asymmetric stretching vibrations appeared at 1322 cm^{-1}. The band between 1587 and 1489 cm^{-1} represented the region for benzene ring stretching. Asymmetric C—O stretching vibrations appeared at 1244 and 1014 cm^{-1}. The symmetric deformation associated with the CH_3—C—CH_3 group was found in the region 1364 and 1410 cm^{-1}. Similarly, in the case of PI spectra, the symmetric and asymmetric stretchings of the C=O group were observed at 1710 and 1782 cm^{-1}, respectively, whereas a benzophenone carbonyl band was noticed at 1608 cm^{-1}. The peak related to C=C stretching of the aromatic ring was observed at 1510 cm^{-1}. C—N—C axial vibrations were observed in the region 1210–1389 cm^{-1}, whereas transverse stretching vibrations were found at 1028 cm^{-1}. The band observed at 1144 cm^{-1} was ascribed to the presence of C_6H_4. The peak due to aromatic ring bending vibrations was observed at 833 cm^{-1}. The stretching vibrations due to C—C=O bonds occurred at 684 cm^{-1}. These observations were in good agreement with previous studies.[29–34] In comparison to pure polymers, various spectral shifts of the blended PSF/PI-20% membrane in terms of wave number were observed. For symmetric and asymmetric carbonyl groups for PI, spectral shifts were observed from 1710 to 1717 cm^{-1} and from 1782 to 1773 cm^{-1}, respectively; for C—N—C axial vibrations, the shift was observed from 1210 to 1206 cm^{-1}, whereas the peak at 1389 cm^{-1} remained

TABLE II
Summary of the FTIR Spectral Assignments

Spectral assignment	PSF wave number (cm^{-1})	Membrane blend wave number (cm^{-1})
C_6H_6 ring stretching	1489–1587	1495–1584
CH_3—C—CH_3 symmetric stretching	1410,1364	1406, 1364
C—O asymmetric stretching	1244, 1014	1247, 1014
S=O symmetric stretching	1307, 1150	1303, 1151
C—SO_2—C asymmetric stretching	1322	1322
Spectral assignment	PI wave number (cm^{-1})	Membrane blend wave number (cm^{-1})
C=O symmetric and asymmetric stretching	1710, 1782	1717, 1773
C—N—C axial stretch and transverse stretching	1210–1389	1216–1389
C=C stretching	1510	1510
C_6H_6 ring bending	833	833

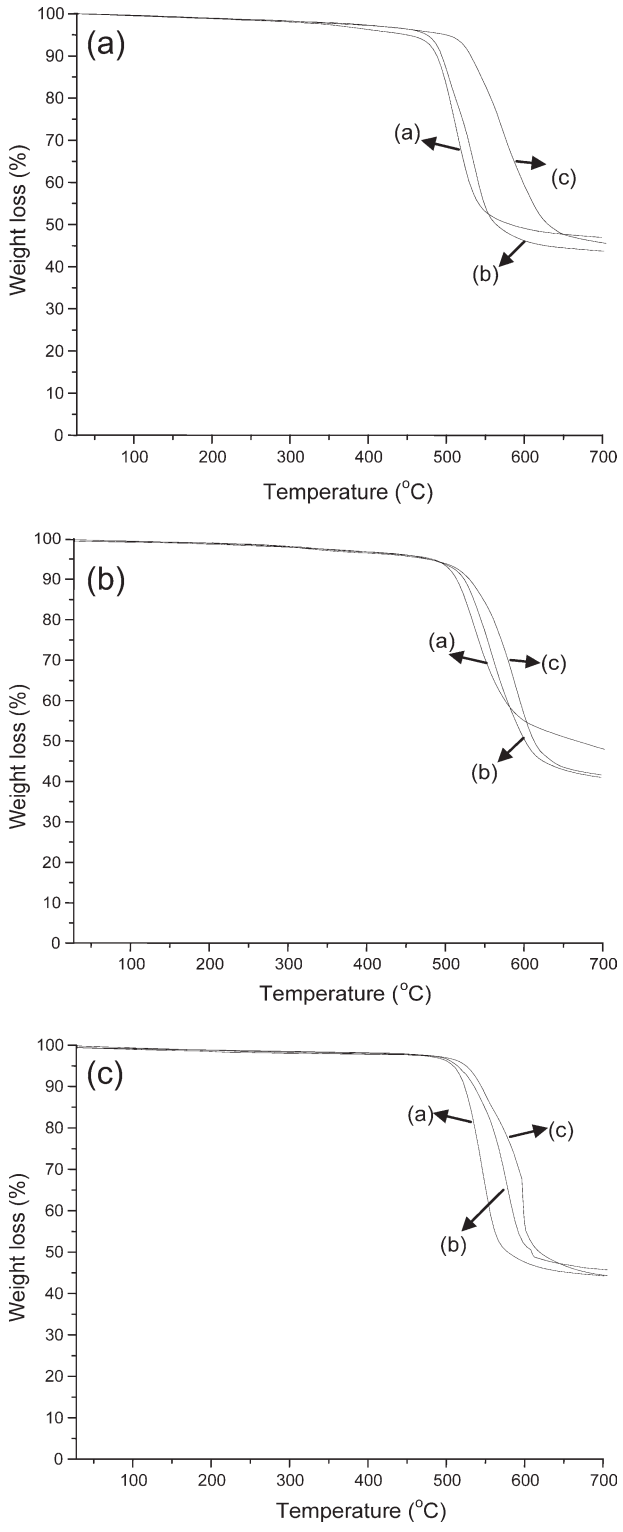

Figure 5 TG curves of (i) PSF, (ii) PSF/PI-10%, and (iii) PSF/PI-20% with heating rates for each at (a) 5, (b) 10, and (c) 15°C/min.

unchanged. Spectral shifts were observed for benzene ring of PSF (from 1587 to 1584 $cm^{-1}$and from 1489 to1495 cm^{-1}) for the respective symmetric and asymmetric vibrations of S═O (from 1150 to 1151 cm^{-1} and from 1307 to 1303 cm^{-1}), for asymmetric vibrations of C—O (from 1244 to 1247 cm^{-1}), and for symmetric vibrations of CH_3—C—CH_3 group deformation (from 1410 to 1406 cm^{-1}). The summarized form of different shifts in the FTIR spectra, as presented in Table II, supported the development of some interactions among the polymers; this indicated their compatibility in the form of blended membranes.[35]

TG studies of the samples were carried out at three different heating rates, and they were intentionally kept at relatively higher values, for example, 5, 10, and 15°C/min, to gather the insight into the degradation process under practically simulated conditions.[36] Only one range of thermal degradation temperatures was observed for all of the compositions; this supported the proper miscibility of the phases. A few typical TG traces for the thermal degradation of the polymeric membranes are presented in Figure 5. The values for the degradation onset temperature and the maximum degradation temperatures for all of the compositions at different heating rates are reported in Table III. It could be seen that with the increase in PI content in the composition, the peak temperature for the degradation increased from 510 to 600°C (Fig. 6). This increase in the peak temperature could have been related to the effect of heat transfer in the material.[37] It might have been correlated to the enhanced crosslinking of the polymers with the increase in PI content, which resulted in the improvement in the thermal stability.[38,39] The presence of a single decomposition peak could have been related to the homogeneity of the samples.

The kinetics of the thermal degradation process was studied for proper understanding of the degradation for developed membranes. If we assumed a solid-to-gas phase transformation during the degradation process, the general reaction during the heat treatment could be represented in the following way:

$$\mathrm{A\,(solid)} \rightarrow \mathrm{B(solid)} + \mathrm{C(Gas)} \tag{1}$$

The fractional conversion (α) for the degradation process can be presented in the following way in terms of the weight changes during the thermal treatment:

$$\alpha = \frac{w_0 - w_t}{w_0 - w_f} \tag{2}$$

where w_0 is the initial weight of dry sample, w_t is the actual mass of the sample at instant t, and w_f is the final weight of the sample at the end of TGA.

The isothermal degradation rate ($d\alpha/dt$) can be presented as a product of the rate constant [$K(T)$], and a function of the conversion [$f(\alpha)$] in the following way:

TABLE III
Dynamic TG Data and E_a Values of Various PSF/PI Blends

Membrane	β (= dT/dt (°C/min)	Degradation onset temperature (°C)	Maximum degradation temperature (°C)	E_a (kJ/mol)	A	n
PSF	5	485	510	206.1849	4472.698	1
	10	497	533			
	15	526	567			
PSF/PI-5%	5	498	520	211.4598	3323.419	
	10	509	537			
	15	534	572			
PSF/PI-10%	5	511	537	225.3002	3847.777	
	10	528	557			
	15	545	583			
PSF/PI-15%	5	522	544	237.5732	3170.044	
	10	537	560			
	15	556	585			
PSF/PI-20%	5	535	549	253.1729	1083.825	
	10	548	568			
	15	567	600			

$$\frac{d\alpha}{dt} = K(T)f(\alpha) \tag{3}$$

$K(T)$ can be expressed by the Arrhenius equation as follows:

$$K(T) = Ae^{-\frac{E_a}{RT}} \tag{4}$$

where A is the pre-exponential factor, R is the gas constant, and T is temperature of decomposition.

If we combine eqs. (3) and (4), we get

$$\frac{d\alpha}{dt} = Ae^{-\frac{E_a}{RT}}f(\alpha) \tag{5}$$

With β as the heating rate

$$\beta = {}^{dT}/_{dt} \tag{6}$$

If we combine eqs. (5) and (6), we get

$$\beta\frac{d\alpha}{dT} = Ae^{-\frac{E_a}{RT}}f(\alpha) \tag{7}$$

Taking the logarithm of both sides, we get

$$\ln(\beta\frac{d\alpha}{dT}) = \ln[Af(\alpha)] - \frac{E_a}{RT} \tag{8}$$

Therefore, a linear plot of the left-hand side against $1/T$ would enable us to evaluate the value of E_a from the slope.[40] Typical linearized plots are presented in Figure 7, and the evaluated E_a values for the different compositions are presented in Table III. From the results, it is evident that with the increase in the PI content in the PSF matrix, E_a for the degradation of the polymer composites increased significantly; this indicated an improvement in the thermal stability of the composites.

Again, if we assume an order-based reaction mechanism operating during the thermal degradation of the polymers, the kinetic function $f(\alpha)$, which actually describes the mechanism of the degradation process, can be represented in terms of the fractional degradation in the following way:

$$f(\alpha) = (1-\alpha)^n \tag{9}$$

where n is the order of the degradation reaction.

Equation (8) can now be presented in the following way:

$$\ln(\beta\frac{d\alpha}{dT}) = \ln[A(1-\alpha)^n] - \frac{E}{RT} \tag{10}$$

Equation (10) can be simplified in the following form:

$$\ln(\beta\frac{d\alpha}{dT}) = (\ln A - \frac{E}{RT}) + n\ln(1-\alpha) \tag{11}$$

Therefore, a linear plot of the left-hand side against $\ln(1-\alpha)$ enabled us to evaluate the value of n from the slope and A from the intercept. The results are presented in Table III. It can be seen that the thermal degradation of the polymeric blends mostly followed first-order kinetics; this indicated that the rate of the degradation process was proportional to the concentration of the undegraded species. Values of A, which indicate the number of thermally activated species, were also found to exist in a similar range for all of the compositions, except in the batch containing the maximum proportion of PI. This indicated an enhanced degree of thermal

stability for the composition with the maximum amount of PI.

SUMMARY AND CONCLUSIONS

Asymmetric PSF/PI blended polymeric membranes were fabricated by a phase-inversion technique. The polymeric constituents showed adequate compatibility, as indicated by the existence of a single T_g. The kinetics of thermal degradation for these membranes were studied with TG. The degradation reactions could be described by first-order kinetics, and E_a of the degradation increased with the increase in the PI content in the composition; this indicated an improvement in the thermal stability with the increase in the PI content in the compositions.

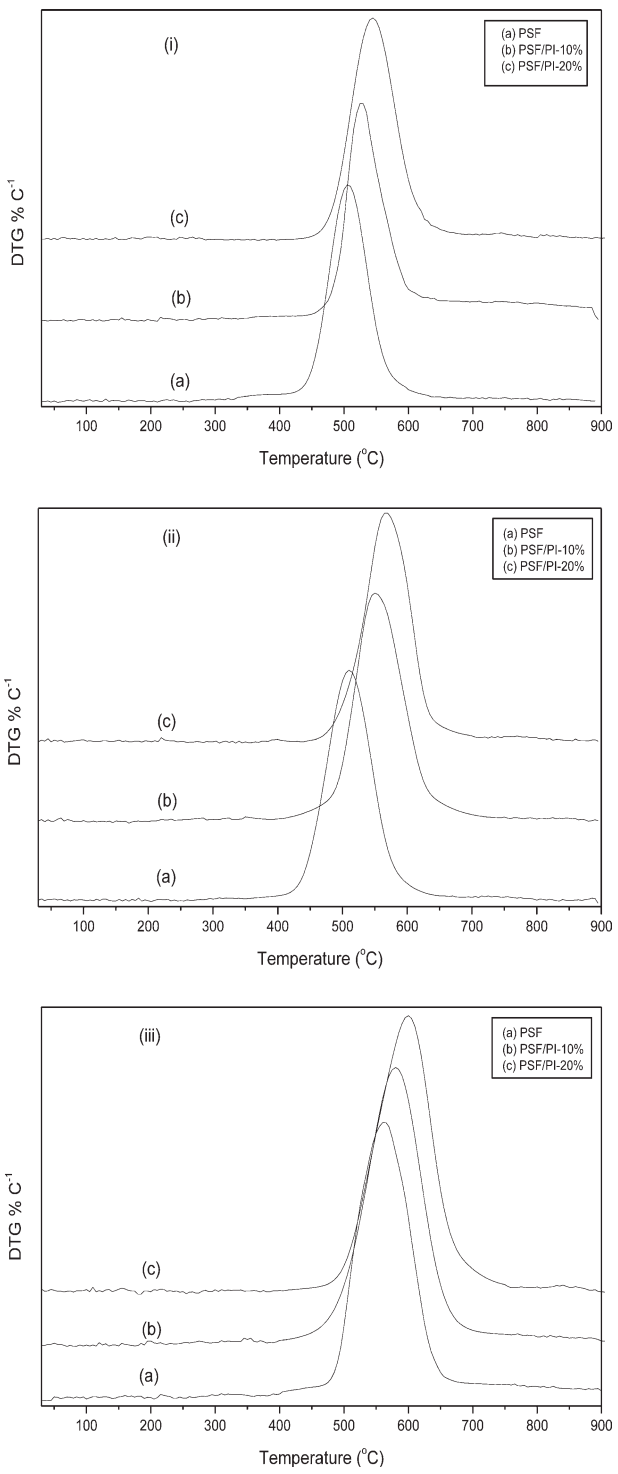

Figure 6 Derivative TG curves of PSF, PSF/PI-10%, and PSF/PI-20% at (i) 5, (ii) 10, and (iii) 15°C heating rates.

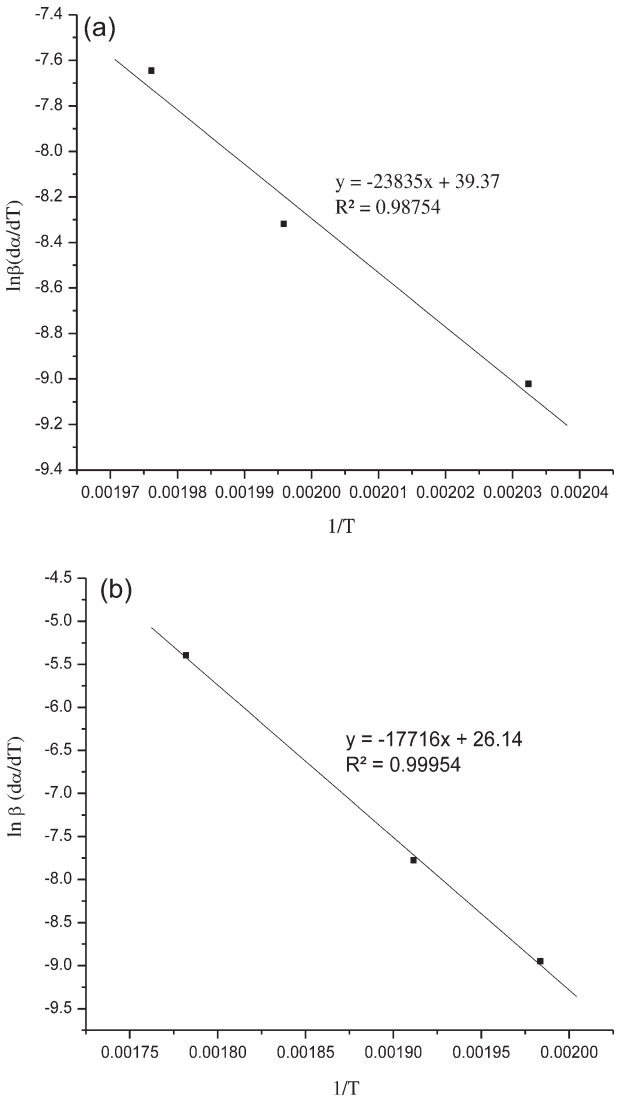

Figure 7 Linear plots of ln $\beta(d\alpha/dt)$ versus $1/T$: (a) PSF/PI-10% and (b) PSF/PI-20% at same α values (0.01).

References

1. Yilmaz, G.; Toiserkani, H.; Dermirkol, D. O.; Sakarya, S.; Timur, S.; Yagci, Y.; Torun, L. J Appl Polym Sci 2010, 49, 110.
2. Nagarale, R. K.; Gohil, G. S.; Shahi, V. K. Adv Colloid Interface Sci 2006, 119, 97.
3. Sur, G. S.; Sun, H. L.; Lyu, S. G.; Mark, J. E. Polymer 2001, 42, 9783.
4. Hwang, J. W.; Cho, K.; Yoon, T. H.; Park, C. E. J Appl Polym Sci 2000, 77, 921.

5. Rahimpour, A.; Madaeni, S. S. J Membr Sci 2007, 305, 299.
6. Sivakumar, M.; Mohan, D.; Rangarajan, R. J Membr Sci 2006, 268, 208.
7. Ghosh, A.; Banerjee, S. J Appl Polym Sci 2008, 109, 2329.
8. Wang, K.; Liou, W.; Liaw, D.; Huang, S. Polymer 2008, 49, 1538.
9. Rozhanskii, I.; Okuyama, K.; Goto, K. Polymer 2000, 41, 7057.
10. Staudt-Bickel, C.; Koros, W. J. J Membr Sci 2000, 170, 205.
11. Mehdipour-Ataei, S.; Amirshaghaghi, A. J Appl Polym Sci 2005, 96, 570.
12. Kim, T.-H.; Koros, W. J.; Husk, G. R. J Membr Sci 1989, 46, 43.
13. Lisa, G.; Avram, E.; Paduraru, G.; Irimia, M.; Hurduc, N.; Aelenei, N. Polym Degrad Stab 2003, 82, 73.
14. Bormashenko, E.; Pogreb, R.; Sheshnev, A.; Shulzinger, E.; Bormashenko, Y.; Sutovski, S.; Pogreb, Z.; Katzir, A. Polym Degrad Stab 2001, 72, 125.
15. Adamczak, A. D.; Spriggs, A. A.; Fitch, D. M.; Awad, W.; Wilkie, C. A.; Grulan, J. C. J Appl Polym Sci 2010, 115, 2254.
16. Ren, L.; Fu, W.; Luo, Y.; Lu, H.; Jia, D.; Shen, J.; Pang, B.; Ko, T.-M. J Appl Polym Sci 2004, 91, 2295.
17. Totu, E.; Segal, E.; Covington, A. K. J Therm Anal Calorim 1998, 52, 383.
18. Large, L. G.; Delgado, P. G.; Kawano, Y. J Therm Anal Calorim 2004, 75, 521.
19. Molnar, G.; Botyay, A.; Poppl, L.; Torkos, K.; Borossay, J.; Mathe, A.; Torok, T. Polym Degrad Stab 2005, 89, 410.
20. Li, X. G.; Huang, M. R. React Funct Polym 1999, 42, 59.
21. Friedman, H. L. J Polym Sci Part C: Polym Symp 1964, 6, 183.
22. Aroon, M. A.; Ismail, A. F.; Motazer-Rahmati, M. M.; Matsuura, T. Sep Purif Technol 2010, 72, 194.
23. Leblanc, N.; Cerf, D. L.; Chappey, C.; Langevin, D.; Metayer, M.; Muller, G. Gas Sep Purif 2001, 22–23, 277.
24. Pesek, S.; Koros, W. J. J Membr Sci 1994, 88, 1.
25. Sharpe, I. D.; Ismail, A. F.; Shilton, S. J Sep Purif Technol 1999, 17, 101.
26. Shilton, S. J.; Ismail, A. F.; Gough, P. J.; Dunkin, I. R.; Gallivan, S. L. Polymer 1997, 38, 2215.
27. Krishnamoorthy, L.; Arif, P. M.; Ahmedkhan, R. J Mater Sci 2011, 46, 2914.
28. Krause, B.; Diekmann, K.; van der Vegt, N. F. A.; Wessling, M. Macromolecules 2002, 35, 1738.
29. Wahab, M. A.; Kim, I. I.; Ha, C.-S. Polymer 2003, 44, 4705.
30. Sridhar, S.; Veerapur, R. S.; Patil, M. B.; Gudasi, K. B.; Aminabhavi, T. M. J Appl Polym Sci 2007, 106, 1585.
31. Sridhar, S.; Smitha, B.; Mayor, S.; Prathab, B.; Aminabhavi, T. M. J Mater Sci 2007, 42, 9392.
32. Barsema, J. N.; Klijnstra, S. D.; Balster, J. H.; van der Vegt, N. F. A.; Koops, G. H.; Wessling, M. J Membr Sci 2004, 238, 93.
33. Raslan, R.; Mohammad, A. W. J Appl Sci 2010, 10, 2628.
34. Jiang, L. Y.; Chung, T. S.; Kulprathipanja, S. J Membr Sci 2006, 276, 113.
35. Linares, A.; Acosta, J. L. J Appl Polym Sci 2004, 92, 3030.
36. Gracia-Fernandez, C. A.; Gomez-Barreiro, S.; Ruiz-Salvador, S.; Blaine, R. Prog Org Coat 2005, 54, 332.
37. Volker, S.; Rieckmann, T. J Anal Appl Pyrolysis 2002, 62, 165.
38. Xiao, C.; Weng, L.; Zhang, L. J Appl Polym Sci 2002, 84, 2554.
39. Muraki, T.; Ueta, M.; Ihara, E.; Inoue, K. Polym Degrad Stab 2004, 84, 87.
40. Lin, J.; Chang, Y. C.; Wu, H. C.; Shih, M. S. Polym Degrad Stab 1996, 53, 295.